Quantum Nuclear *ab Initio* Molecular Dynamics Study of Water Wires

Hsiao S. Mei,[†] Mark E. Tuckerman,[‡] Diane E. Sagnella,[§] and Michael L. Klein*,[†]

Center for Molecular Modeling and Department of Chemistry, University of Pennsylvania, Philadelphia, Pennsylvania 19104-6323, Department of Chemistry, New York University, New York, New York 10003, and Department of Chemistry, Boston University, Boston, Massachusetts 02215

Received: June 15, 1998

The structure of linear water wires with an excess proton was studied at room temperature using *ab initio* path integral molecular dynamics. The *ab initio* Car−Parrinello (CP) methodology employed the density functional theory (DFT) description of the electronic structure, and the Feynman path integral approach allowed for quantization of the nuclear degrees of freedom. Thus, the influence of proton tunneling and zero point nuclear vibrations were automatically included. Four or five water molecules were linearly arranged, with an excess proton (H*), to form tetramer and pentamer complexes, respectively. In classical studies of the tetramer complex, the excess proton H*, centered within the wire, formed H_3O^+ and $H_5O_2^+$ ions with the two inner water molecules. In the pentamer complex, the H* was found attached to the inner water molecule, forming a stable H_3O^+ ion with two covalent, hyperextended bonds that were hydrogen bonded to neighboring water molecules on both opposite sides. Although the addition of nuclear quantization via path integrals broadened the calculated distribution functions for both complexes, the overall features were unaltered, which suggests that nuclear quantum effects are minimal in these small, linear clusters. However, instantaneous path integral configurations revealed the formation of an extended $H_7O_3^+$ complex predominantly in the pentamer wire, where the excess proton H* was delocalized over three adjacent water molecules simultaneously. Since the computational demands of CP make long simulations cost-prohibitive, angular distribution functions, requiring much longer simulation times, were obtained using an MP2-based empirical valence bond (EVB) model [Sagella, D. E.; Tuckerman, M. E. *J. Chem. Phys.* **1998**, *108*, 2073]. Additional classical CP calculations, where the water wire ends were solvated with additional capping waters, were also performed. In these studies, the proton was observed to be much more mobile; proton transfer occurred along the full water wire and occasionally into the water solvation caps.

I. Introduction

Certain proteins mediate proton translocation[1] across biological membranes and therefore establish an electrochemical potential gradient, which provides energy to fuel essential processes within the cell.[2] Thus, the study of proton transfer broadens our comprehension of how proteins, such as bacteriorhodopsin of *Halobacterium*, F_0/F_1 ATP synthase, and cytochrome *c* oxidase, mediate the translocation process and gives insight into basic cellular functions such as ATP synthesis and cell locomotion. Water is known to play a role in the translocation process by forming a hydrogen-bonded chain, to serve as a pathway for the proton. These quasi one-dimensional pathways, named "proton wires" or "water wires" are thought to constitute the basic structure of the hydrogen-bonded chain (HBC) mechanism,[3] where protons hop along a hydrogen-bonded network in response to local network conformational changes, thus producing a charge translocation. This is similar to the picture of the Grötthuss proton shuttling mechanism in water and ice.

Experimental studies in the photosynthetic reaction center (RC), which mediates light driven electron−proton transfer reactions during photosythesis, from purple bacteria *Rhodobacter spaeroides*[4−6] and *Rhodopseudomanas viridis*[5,7] have shown the presence of water wire channels (named P1 and P2) composed of >10 H_2O units, between the secondary quinone Q_B pocket (involved in electron transfer to Q_B^-) and the aqueous cytoplasm. In the most recent report regarding *Rb. spaeroides*,[4] water pathway P2 was identified in addition to the previously known pathway P1.[5,6] The P1 and P2 pathways run from the Q_B pocket in directions perpendicular and parallel to the membrane surface, respectively, and the P2 pathway ends near the surface of the membrane, while P1 extends and then terminates farther into the cytoplasmic region. These water wire pathways are believed to conduct protons, since proton transfer rates are observed to be reduced when the P1 channel is partially blocked;[8] the waters may also serve to facilitate the release of protonated quinone, ubiquinol, from the Q_B pocket. These processes may contribute to the creation of a proton gradient across the membrane, which drives ATP synthesis.

Shorter water wires, composed of <10 H_2O units, have also been experimentally identified in three biological systems[9−11] of interest. Gramicidin A (gA) holds linear water wires of about 9 H_2O units[9] and has been used as a model of proton conduction

[†] University of Pennsylvania.
[‡] New York University.
[§] Boston University.

10.1021/jp982623t CCC: $15.00
Published on Web 11/20/1998

in F_0/F_1 ATP synthase,[12,13] since the process in the synthase is unknown but is believed to be similar to that found in the gA channel. Cytochrome *f*, a subunit of cytochrome b_6f holds an L-shaped bidirectional water channel composed of five H_2O units (with four H_2O molecules residing in the longer channel direction);[10] this small water chain has been proposed to function as an exit port for proton translocation from the cytochrome b_6f integral membrane protein complex, which is responsible for electron transfer between two RC photosynthetic membranes. In bacteriorhodopsin, four[11] to eight[14] water molecules have been found in the proton channel close to the Retinal and Schiff base and may be involved in proton translocation during the photocycle.

Theoretical studies have primarily investigated water wires in vacuum[15−18] or within an ion channel gA[19−23] where chemical dissociation was either precluded or included based upon the methodology used. Although the majority of the aforementioned studies have focused on H^+ transfer, the role of gA as a monovalent transmembrane ion channel has been well studied previously.[24] In the nondissociative model water studies, the structure of pure water[19] or hydronium H_3O^+ solvated by the water wire[22] in gA was examined while, in the dissociative studies, an excess proton H^+ was placed within the water wire and either semi-empirical effective model potentials[15,16,20,21] or *ab initio* methods[23] were used to study equilibrium and dynamical properties of proton transfer. Electric fields have also been imposed on these model water wires to study nonequilibrium quantum dynamics using combined *ab initio* and semi-empirical methods.[17,18]

In the *ab initio* Car−Parrinello (CP)[25] studies, a water wire was embedded within a polyglycine gA[23] and it was observed that internal carbonyl groups, which line the interior of the channel acted as hydrogen bonding sites to small charged water complexes (such as H_3O^+ and $H_5O_2^+$). It was proposed that these sites, which complete a "solvation" shell of the charged complexes, mediated proton transfer along the water wire. The "solvation" of water wires, through hydrogen bonds to the channel carbonyl groups, was also observed in earlier nondissociative studies of water solvation in the gA channel.[22]

Pomès and Roux have previously allowed for nuclear quantization in their study of water wires in vacuum[15,16] and within the ion channel gA.[20,21] These authors relied on a fully dissociative, polarizable effective potential PM6[26,27] to model proton transfer. Among the problems associated with the PM6 potential are its inability to model condensed phase environments[28] and overestimation of proton transfer barriers. Pomès and Roux have addressed the first shortcoming[15,16] but, owing to the latter, found quantum nuclear dispersion to be significant. In their purely classical studies, they found that the removal of hydrogen bonding between the water wire and ion channel caused a dramatic increase in proton mobility within the channel.

The *ab initio* CP[25] molecular dynamics (MD) method employed in this work does not rely on empirical potential functions but obtains internuclear forces from an "on the fly" density functional theory (DFT) based electronic structure calculation. DFT calculations of the geometries and energetics of charged water complexes in the gas phase have shown good agreement with high level electronic structure calculations.[29] In addition, DFT based *ab initio* MD calculations of pure water[30,31] and of proton transfer in water both at 300 K[32,33] are in good agreement with experiment[34−36] Nuclear quantum effects at finite temperature are incorporated into CP via the Feynman imaginary time path integral formulation of quantum statistical mechanics (PICP),[37,38] whereby it is possible to investigate the influence of tunneling and zero point vibrations on equilibrium properties at finite temperatures and still maintain an *ab initio* determination of the electronic structure.[39−41] Applications of the PICP MD method to studies of hydrogen chloride crystal hydrates, charged water complexes in the gas phase, fluxional molecules, and high-pressure ice have already been presented.[29,42−45]

For the linear water wires, it is of interest to provide a more realistic modeling of bond breaking and formation during proton transfer[23,30,32,31,33,46,47] than the PM6 model can provide, while investigating the importance of nuclear quantum corrections via path integrals.[29,42] Accordingly, we have undertaken the study of an excess proton within linear water wires using CP and PICP methods. Following previous work by Pomès and Roux,[15,16] the charged water wire has been placed within a vacuum environment; an external cylindrical constraining potential has been added to maintain the single-stranded linear character of the water chain. This work has neglected solvation effects from the channel environment and nonequilibrium effects, such as applied electric fields,[17,18] and has instead focused on the equilibrium effects of nuclear quantization in a simple, but relevant model. Studies have been performed using different parameters for the cylindrical constraining potential. Capping solvation effects, from additional water added to solvate the water wire ends, have also been studied. As noted earlier, the biological environment can influence the proton transfer process, and such an investigation will be reserved for future PICP studies.

II. Methods

A. *Ab Initio* CP and PICP Molecular Dynamics. The CP methodology employs a DFT description of electronic structure and is based on the Hohenberg−Kohn variational principle.[48] This states that the ground state electronic energy E_0

$$E_0 = \min_{\{\phi_i\}} E[\{\phi_i\},\{\mathbf{R}_I\}] \tag{1}$$

is the minimum of the the Kohn−Sham (KS) energy functional $E[\{\phi_i\},\{\mathbf{R}_I\}]$, which is a function of KS orbitals $\{\phi_i\}$ and nuclear $\{\mathbf{R}_I\}$ degrees of freedom and has the form[49]

$$E[\{\phi_i\},\{\mathbf{R}_I\}] = -\frac{1}{2}\sum_i \langle\phi_i|\nabla^2|\phi_i\rangle + \frac{1}{2}\int\int d\mathbf{r}\, d\mathbf{r}'\frac{n(\mathbf{r})\, n(\mathbf{r}')}{|\mathbf{r}-\mathbf{r}'|} + E_{xc}[n] + \int d\mathbf{r}\, n(\mathbf{r})\, V_{loc}(\mathbf{r},\{\mathbf{R}_I\}) + \sum_i \langle\phi_i|\hat{V}_{NL}(\{\mathbf{R}_I\})|\phi_i\rangle + \sum_{I<J}\frac{Z_I Z_J}{|\mathbf{R}_I-\mathbf{R}_J|} \tag{2}$$

where atomic units have been employed. The minimization is carried out subject to an orthonormality constraint where $\langle\phi_i|\phi_j\rangle = \delta_{ij}$. The above equation gives the electron density $n(\mathbf{r}) = \sum_i|\phi_i(\mathbf{r})|^2$ as a sum over occupied states *i*. It also includes terms for the kinetic and Hartree energies, electron exchange, and correlation functional E_{xc}, local V_{loc} and nonlocal V_{NL} pseudopotential contributions, and ion−ion Coulombic energies, respectively. The required basis set is reduced in size by the use of atomic pseudopotentials, which eliminate the core electrons. Thus the KS orbitals $\{\phi_i\}$ give the electronic structure of the valence electrons in the field of classical ions $\{\mathbf{R}_I\}$, which consist of both nuclei and attached core electrons.

Rather than relying on a traditional self-consistent method to solve the KS equations $\hat{H}_{KS}|\phi_i\rangle = \epsilon_i|\phi_i\rangle$, the ground state density n_0 and KS orbitals $\{\phi_i\}$ can be obtained by using the CPMD method.[25] In CPMD, an extended Lagrangian is formulated as

$$L = \mu\sum_i\langle\dot{\phi}_i|\dot{\phi}_i\rangle + \frac{1}{2}\sum_I M_I\dot{\mathbf{R}}_I^2 - E[\{\phi_i\},\{\mathbf{R}_I\}] + \sum_{i,j}\Lambda_{ij}(\langle\phi_i|\phi_j\rangle - \delta_{ij}) \quad (3)$$

The first term in eq 3 corresponds to a fictitious kinetic energy with fictitious mass parameter μ (having units of energy·time^2), and M_I is the classical ionic mass of ion I. The final term in eq 3, which involves a set of Lagrange multipliers Λ_{ij}, is used to impose the orthonormality condition on the orbitals.[50−53]

MD equations of motion for the classical ions $\{\mathbf{R}_I\}$ and KS orbitals $\{\phi_i\}$ are derived from the Lagrangian in eq 3.[53] The ions $\{\mathbf{R}_I\}$ evolve from both Coulomb ion−ion forces and Hellman−Feynman force contributions from the KS energy functional. The KS orbitals $\{\phi_i\}$ execute a fictitious adiabatic "dynamics" that allows them to follow the nuclear motion and fluctuate with small amplitude about the exact ground state surface. The electronic adiabaticity is maintained through the use of Nosé−Hoover chain thermostats,[54] in a "knotted" chain scheme,[53,55] and through the choice of μ, whereby the fictitious kinetic energy is kept small compared to that of the nuclei while allowing the electrons to move rapidly in response to nuclear displacements.[53,56,57]

Recent advances in *ab initio* molecular dynamics have included approximate nuclear quantum corrections.[29,39−41,42,58] In the limit where thermal fluctuations are small compared to the electronic energy gap, PICPMD can be used: the nuclei are quantized via the Feynman path integral[37,38] while the electronic degrees of freedom remain on the adiabatic ground state surface E_0. Path integration yields the canonical partition function $Z(N,V,T)$ for a system of N total ions in a volume V at temperature T.

$$Z(N,V,T) = \lim_{P\to\infty}\left[\prod_{I=1}^{N} N\int d\mathbf{R}_I^{(1)}\ldots d\mathbf{R}_I^{(P)}\int d\mathbf{P}_I^{(1)}\ldots d\mathbf{P}_I^{(P)}\right]\times \exp\left[-\beta\sum_{s=1}^{P}\left(\sum_{I=1}^{N}\left\{\frac{(\mathbf{P}_I^{(s)})^2}{2M_I'} + \frac{1}{2}M_I\omega_P^2(\mathbf{R}_I^{(s)} - \mathbf{R}_I^{(s+1)})^2\right\} + \frac{1}{P}E_0(\{\mathbf{R}_I^{(s)}\})\right)\right] \quad (4)$$

In practice, P is chosen large but finite and cyclic boundary conditions apply so that the index $P + 1 = 1$. Thus, each quantum particle is represented as a cyclic polymer chain with P points or "beads" connected by harmonic springs.[59,60] In eq 4 above, N is an appropriate normalization constant, and ion I at imaginary time slice (s) has position $\mathbf{R}_I^{(s)}$, fictitious momenta $\mathbf{P}_I^{(s)}$, fictitious mass M_I', and ω_P is the bead frequency given by $\sqrt{P}/\beta$, where β is the inverse temperature. The ground state energy $E_0^{(s)}$ corresponds to the minimum of the KS energy functional $E[\{\phi_i\}^{(s)},\{\mathbf{R}_I\}^{(s)}]$ at imaginary time slice (s).

The conjugate momenta for the ions $\mathbf{P}_I^{(s)}$ have been explicitly introduced in eq 4[59] (as $3NP$ uncoupled Gaussian integrals) to be used in a PICP algorithm where the extended Lagrangian is[39−41]

$$L = \sum_{s=1}^{P}\left\{\frac{\mu}{P}\sum_i\langle\dot{\phi}_i^{(s)}|\dot{\phi}_i^{(s)}\rangle + \frac{1}{2}\sum_I M_I'(\dot{\mathbf{R}}_I^{(s)})^2 - \frac{1}{2}M_I\omega_P^2(\mathbf{R}_I^{(s)} - \mathbf{R}_I^{(s+1)})^2 - \frac{1}{P}E[\{\phi_i\}^{(s)},\{\mathbf{R}_I\}^{(s)}] + \frac{1}{P}\sum_{i,j}\Lambda_{ij}^{(s)}(\langle\phi_i^{(s)}|\phi_j^{(s)}\rangle - \delta_{ij})\right\} \quad (5)$$

Above in eq 5, the PICP Lagrangian terms are similar to the ordinary CP Lagrangian L in eq 3. However, the PICP Lagrangian is discretized over imaginary time slices (s) and the third term on the right hand side of eq 5 is the harmonic bead interaction from the nuclear quantum kinetic energy. MD equations of motion can be derived from the PICP L and are given in refs 40 and 41. Although MD equations of motion are derived, the dynamics are fictitious and sample the appropriate thermal distribution of nuclear quantum states; real time dynamical properties, such as rates of quantum proton transfer, cannot be obtained by these methods. As described in refs 40 and 41, the stiff harmonic springs, with chain frequencies ω_P, make efficient sampling of the path integral quantum distribution functions difficult using standard MD techniques.[61] Algorithms have been devised to handle such problems. These employ MD staging transformations[40,62] based upon the path integral staging Monte Carlo algorithm,[63−66] normal mode transformations,[40] and the thermostating of each staging or normal mode degree of freedom;[40,53,55] the interested reader is referred to these cited references for further details.

B. Computational Details. An excess proton was studied within four and five member water wires (hereafter named the "tetramer" and "pentamer" complexes, respectively). These two different length wires were chosen mainly to investigate how the imposed symmetry of the water chain affects its equilibrium properties. Previous work has suggested that in the tetramer complex, the excess proton is located in the geometric center of the complex, while in the pentamer complex, the excess proton binds to the midchain water molecule to form a hydronium ion centered within the water wire.[15,16]

An instantaneous configuration of the thermally equilibrated water wire was taken from a classical MD simulation of the hydrated transmembrane gA ion channel at 300 K where the excess proton was present as hydronium ion H_3O^+ and approximately centered within the linear chain of water molecules. The isolated complexes were then placed in a "soft potential" of the harmonic form, with a force constant $k = 10$ kcal/mol·Å^2, which confined the oxygens of the system to a cylinder of approximately the same diameter as the gA ion channel.[15,16] This is needed to preserve the quasi one-dimensional character of the chain. Studies were also performed using a larger force constant $k = 130$ kcal/mol·Å^2 in order to harden the potential and emphasize the cylindrical shape. Thus the influence of the chosen force constant k can be investigated. The hard and soft complexes were placed in simulation boxes of dimensions 7 Å × 7 Å × 12 Å and 7 Å × 7 Å × 17 Å for the tetramer and pentamer complexes, respectively; periodic boundary conditions were applied in both cases. Cluster boundary conditions[67] were checked against the periodic boundary conditions with no noticeable differences observed.

Electron exchange and correlation were treated at the generalized gradient approximation (GGA) level[68] using the Becke (B) exchange[69] and Lee, Yang, and Parr (LYP) correlation functionals.[70] The BLYP scheme has been shown to give a good description of aqueous hydrogen bonding[31] and excellent results for intermolecular O−O distances. Moreover, structural findings for small charged water clusters in the gas phase compare well[29]

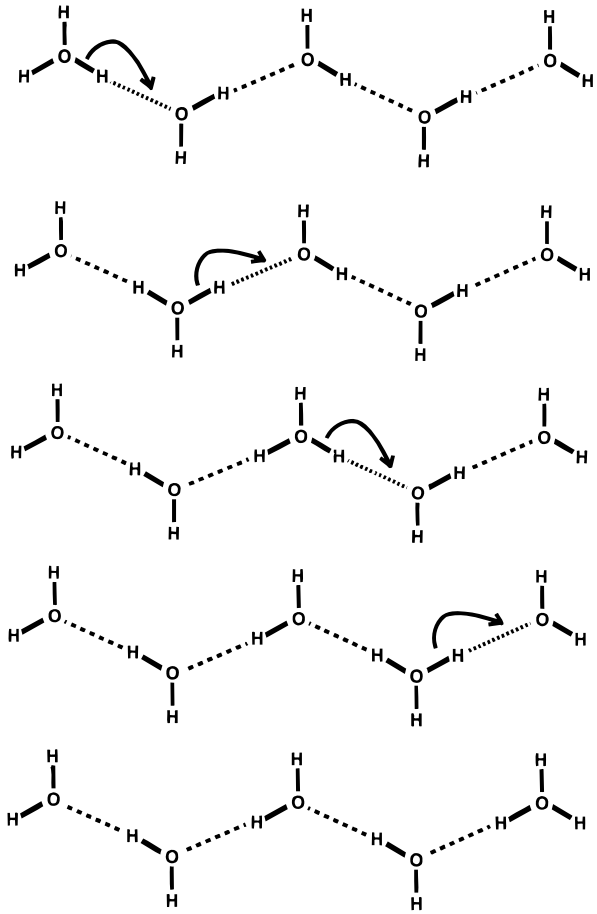

Figure 1. Schematic of a protonated water wire, which, from top to bottom, illustrates consecutive Grötthuss proton hops (arrows) and rearrangement of water dipoles across the wire.

to high-level fully correlated quantum electronic structure calculations.[71] Atomic pseudopotentials of the Troullier and Martins form[72] were used to take into account the effect of the core electrons, and a 70 Rydberg energy cutoff was used in the plane wave expansion of the KS orbitals.

CP and PICP trajectories were run for several picoseconds at a time step of 0.17 fs with the ions and electrons thermostated using Nosé−Hoover chains[29,40] of length 4 at 300 K. The path integral was discretized using $P = 16$ beads, which was shown to be a good choice based on previous studies of charged water clusters,[29,41] and a normal mode transformation[40] was applied to the ions. Fictitious electron masses were assigned to be 600 au for the CP runs and 1100 au for the PICP runs. Trajectories were accumulated for at least 100 000 steps for the classical CP runs and at least 20 000 steps for the quantum PICP runs.

For the capped water wire study, an equilibrium tetramer complex was chosen and capped by eight water molecules (four water molecules at either end); the initial capping geometry was chosen to solvate the end waters in a tetrahedral H-bonding network. Cluster boundary conditions were employed to suppress capping water images and the capped water was placed in a simulation box size of 9 Å × 9 Å × 19 Å. The cylindrical restraining potential was switched off over a heeling length of 1.5 Å in the z channel axis direction and cutoffs at 4.6 and 14.4 Å were chosen at the approximate ends of the tetramer wire. In the capping region, an additional soft harmonic cylindrical potential was added to keep the water caps within a longer distance of 3.5 Å from the channel axis.

Figure 2. Instantaneous configurations of the protonated tetrameric water wire taken from the classical CP calculation at 300 K. (a) The excess proton (H*) is shown bound to a chain water molecule to form classical H_3O^+. (b) The excess proton is equally shared between the two inner water molecules, forming transient $H_5O_2^+$.

III. Results and Discussion

The tetramer and pentamer complexes consist of linearly arranged water molecules with an excess proton. Figure 1 depicts, schematically, a series of successive proton transfers along the wire. Diffusion of hydronium results in a net reversal of molecular water dipoles. Note that the identity change of the proton as it hops along the wire is consistent with the Grötthuss mechanism of proton transfer. At the start of each simulation, the excess proton is located near the geometric center of the water wire. Both CPMD with classical nuclei and PI-CPMD trajectories are then generated from this initial configuration. Several instantaneous snapshots from the simulations are shown in Figures 2−5 and discussed further below.

In the case of the CP tetramer complex, the excess proton (denoted as H*) was sometimes found attached to one of the two inner water molecules, in the form of the hydronium ion H_3O^+, as shown in Figure 2a. The inner H* proton was observed to migrate only between the two inner waters, covalently bonding with either molecule and giving rise to two possible H_3O^+ sites. The $H_5O_2^+$ species was observed only as a transient intermediate species during the proton transfer; see Figure 2b. The symmetry of the water wire about the inner proton is most easily seen in this $H_5O_2^+$ species where the dipoles of the water molecules on either side of the inner proton oppose one another.

Selected configurations taken from the CPMD study of the pentamer complexes are shown in Figure 3. When the excess proton forms an H_3O^+ ion located in the middle of the chain (see Figure 3a), the pentamer is symmetric, with opposing neighboring water dipoles about this middle H_3O^+ ion. The H_3O^+ ion of the pentamer wire is stably solvated in the center of the wire; however, it was observed that the O−H bonds of the H_3O^+ were pulled by the adjacent nearest neighbor (NN)

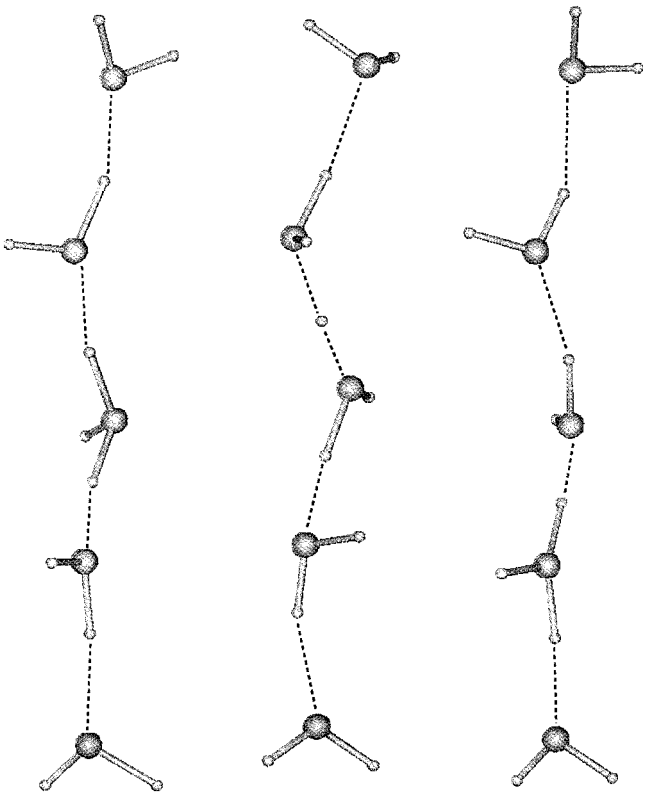

Figure 3. Instantaneous configurations of the protonated pentameric water wire taken from the classical CP calculation at 300 K. (a) The excess proton (H*) forms H_3O^+, which is solvated at the center of the pentamer complex; recall Figure 2. (b) The excess proton is equally shared between two inner water molecules, forming $H_5O_2^+$. (c) The excess proton fully transfers from the middle to the neighboring water molecule to form H_3O^+.

hydrogen-bonded water molecules, thereby creating some proton movement on either side of the inner hydronium ion. During short spans of the simulation, one of the two competing O−H* bonds (H* denoting the H-bonded protons on the H_3O^+ ion) would lengthen toward a NN water to form the transient $H_5O_2^+$ species (see Figure 3b); for the most part the shared H* proton was shortly thereafter drawn back toward the middle water, re-forming the inner H_3O^+ ion. As shown in Figure 3c, full proton transfer to form an off-center NN H_3O^+ ion was possible but, nevertheless, a rare event.

In the PICP runs, discretization of the classical nuclei into beads results in configurations such as those shown shown in Figures 4 and 5. In the case of the PICP tetramer, Figure 4a shows the inner proton beads bonded with the lower water molecule to form a localized quantum H_3O^+ complex. In Figure 4b, the transient path integral $H_5O_2^+$ species is shown. In the PICP pentamer complexes, the proton was found delocalized between two (Figure 5a) or three (Figure 5b) neighboring water sites. Path integral $H_5O_2^+$ structures were observed as well as extended $H_7O_3^+$ where the proton was delocalized over three water sites. These delocalized complexes are particular to the quantum nature of the defect and cannot occur in the classical CP trajectories.

In the classical water chains, proton transfer events were never observed to extend to the end of the water wire. However, in both the PI tetramer and pentamer complexes, the rare event was observed where the excess proton delocalized over the outer

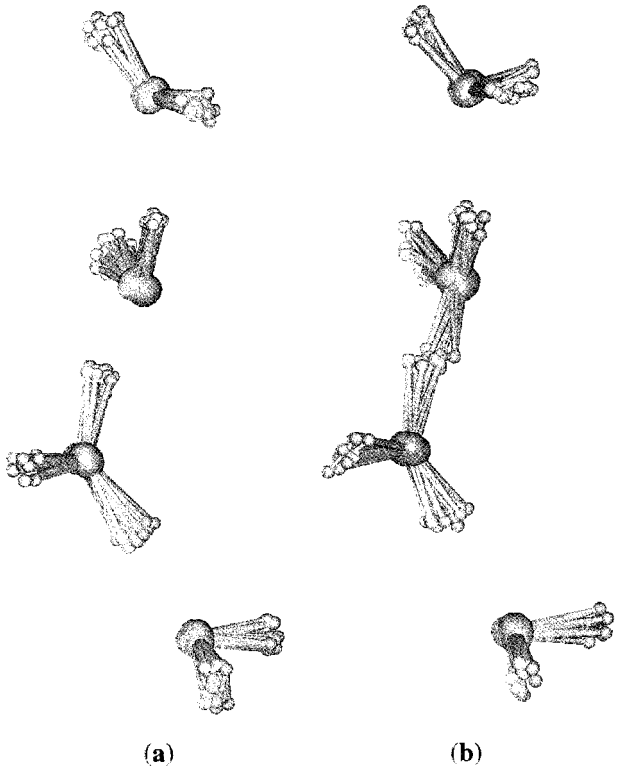

Figure 4. Instantaneous configurations of the protonated tetrameric water wire taken from the PICP calculation at 300 K with $P = 16$ imaginary time slices for each nuclear degree of freedom: (a) the excess proton forming H_3O^+; (b) the excess proton bound to the two inner water molecules, forming quantum $H_5O_2^+$.

three water sites to form the transient $H_7O_3^+$ complex over the end of the chain.

A. Average and Structural Properties. Proton transfer appears to proceed via different mechanisms for each of the complexes. In the tetramer complex, the proton shuttles frequently between the two inner water molecules to form H_3O^+ with either molecule, while in the pentamer complex, the H* protons prefer to remain close to the inner solvated H_3O^+ and full proton transfer to a NN water molecule rarely occurs. Thus, equilibrium properties and the structure of the water wires were calculated to characterize fully the tetramer and pentamer complexes in both the hard and soft channels.

The intermolecular oxygen−oxygen (O−O) pair distances between nearest neighbor waters are calculated for the soft and hard tetramer (T) and pentamer (P) complexes for inner and outer NN O−O pair distances and end to end O−O distances labeled as $R^X_{in}, R^X_{out}, R^X_{end}$, where X = T or P to denote the complex type. The outer pairs are defined as O−O NN pairs from water molecules at the end of the wire, while the inner pairs are the remaining O−O NN pairs near the middle of the wire. These minimum and average values along with statistical root mean square (rms) errors are presented in Table 1 for the hard and soft complexes.

The minimum geometries, shown in Tables 1 and 2, of the soft complexes appear to have more asymmetry than the hard complexes. Especially in the soft tetramer, the geometric minimum possesses a small asymmetry with the proton being located slightly closer to one of the inner water molecules, while in the hard tetramer, the proton was equally shared by the two inner waters, forming $H_5O_2^+$. The two inner waters can penetrate further into the softer cylindrical potential, having a longer inner NN O−O distance of 2.48 Å, while the harder potential constricts the two inner waters to remain closer to the channel

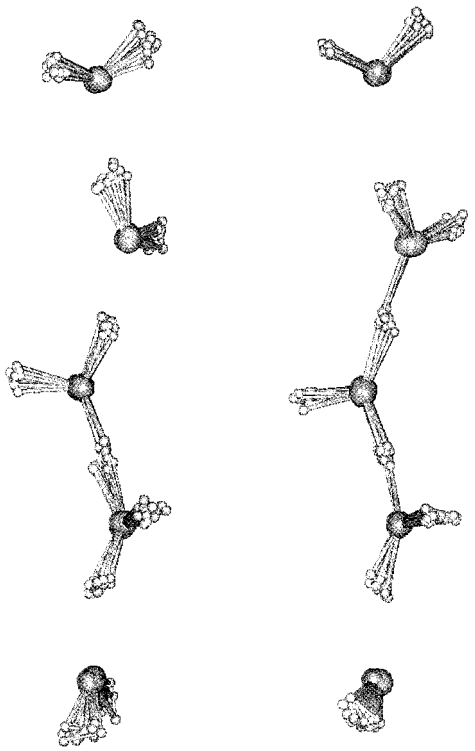

Figure 5. Instantaneous configurations of the protonated pentameric water wire taken from the PICP calculation at 300 K with $P = 16$ imaginary time slices for each nuclear degree of freedom. (a) The excess proton is bound to the two inner water molecules, forming quantum $H_5O_2^+$. (c) The excess proton is delocalized over the middle and two neighboring molecules, forming an extended $H_7O_3^+$.

TABLE 1. Minimum, average CP and PICP Intermolecular Oxygen−Oxygen (O−O) Nearest Neighbor (NN) and End-to-End Distances (Subscript "end") for the Soft and Hard Tetramer (Superscript "T") and Pentamer (Superscript "P") Water Wire Complexes at 300 K[a]

O−O pair distance	minimum potential R_{min}/Å	classical nuclei $\langle R\rangle_C$/Å CP	quantum nuclei $\langle R\rangle_Q$/Å PICP
soft tetramer			
NN R^T_{in}	2.48	2.49 ± 0.01	2.46 ± 0.01
NN R^T_{out}	2.60, 2.64	2.67 ± 0.01	2.63, 2.65 ± 0.02
R^T_{end}	6.78	6.73 ± 0.04	6.74 ± 0.04
soft pentamer			
NN R^P_{in}	2.52, 2.53	2.54 ± 0.01	2.51 ± 0.01
NN R^P_{out}	2.69, 2.71	2.76, 2.77 ± 0.01	2.71 ± 0.02
R^P_{end}	9.26	9.33 ± 0.04	9.26 ± 0.04
hard tetramer			
NN R^T_{in}	2.45	2.48 ± 0.01	2.46 ± 0.01
NN R^T_{out}	2.63, 2.64	2.66, 2.68 ± 0.01	2.63 ± 0.2
R^T_{end}	6.79	6.99 ± 0.03	6.83 ± 0.05
hard pentamer			
NN R^P_{in}	2.51	2.49, 2.50 ± 0.01	2.48, 2.50 ± 0.01
NN R^P_{out}	2.69	2.73, 2.75 ± 0.01	2.68, 2.69 ± 0.01
R^P_{end}	9.35	9.46 ± 0.04	9.35 ± 0.04

[a] NN O−O distances are labeled as inner (subscript "in") and outer (subscript "out") pairs. Statistical rms errors have been calculated using the blocking method.[75] Two tabulated values are given for geometrically asymmetric species.

axis, with a NN O−O separation of 2.45 Å. Thus, the slight elongation of the inner NN O−O distances found in the soft tetramer results in an asymmetric minimum geometry. The differences between minimum geometries for the soft and hard pentamer complexes are less pronounced. In general, the soft complexes can penetrate further into the cylindrical softer confining potential, resulting in a more angular backbone and slightly shorter end-to-end distances, as shown in Table 1.

TABLE 2. Minimum, Average CP and PICP Oxygen−Hydrogen (O−H) Bond Distances for the Hard and Soft Water Wire Tetramer (Superscript "T") and Pentamer (Superscript "P") Water Wire Complexes at 300 K[a]

O−H bond distance	minimum potential r_{min}/Å	classical nuclei $\langle r\rangle_C$/Å CP	quantum nuclei $\langle r\rangle_Q$/Å PICP
soft tetramer			
r^T_{NHB}	0.99	0.99 ± 0.01	0.99 ± 0.01
r^T_{HB*}	1.17, 1.31	1.24, 1.26 ± 0.01	1.24, 1.25 ± 0.01
r^T_{HB}	1.04, 1.05	1.04 ± 0.01	1.05 ± 0.01
soft pentamer			
r^P_{NHB}	0.99	0.99 ± 0.01	0.99 ± 0.01
r^P_{HB*}	1.10, 1.11	1.11, 1.12 ± 0.01	1.13 ± 0.01
r^P_{HB}	1.02	1.02, 1.03 ± 0.01	1.03 ± 0.01
hard tetramer			
r^T_{NHB}	0.99	0.98 ± 0.01	0.99 ± 0.01
r^T_{HB*}	1.22	1.25 ± 0.01	1.24, 1.25 ± 0.01
r^T_{HB}	1.05	1.04 ± 0.01	1.05 ± 0.01
hard pentamer			
r^P_{NHB}	0.99	0.99 ± 0.01	0.99 ± 0.01
r^T_{HB*}	1.10, 1.12	1.10 ± 0.01	1.13, 1.14 ± 0.01
r^P_{HB}	1.02, 1.03	1.01 ± 0.01	1.03 ± 0.01

[a] Bond types: NHB, non-hydrogen-bonded covalent O−H bonds; HB*, hydrogen-bonded O−H* bonds where the proton transfers; HB, hydrogen-bonded covalent O−H bonds (i.e., no proton transfer). Statistical rms errors have been calculated using the blocking method.[75] Two tabulated values are given for geometrically asymmetric species.

Average values from CP and PICP calculations primarily showed that asymmetries in the geometry minima are washed out. Especially in the case of the tetramer, the observed asymmetric minima between the hard and soft channels is absent. With the exception of the end-to-end distances, all CP and PICP soft and hard tetramer average pair distances are within error estimates of one another. For the pentamer, differences between soft and hard potentials were also only significant in the end-to-end distances and in the classical NN inner O−O distances, where the soft pentamer average values were found to be slightly greater.

Differences were seen in the averages obtained from the CP and PICP calculations for both complexes. For the quantum cases, the average O−O lengths are shorter while the average O−H lengths are longer (see Tables 1 and 2). The longer O−H lengths are due to quantum dispersion, which has more of an effect on the lighter protons. The quantum delocalization from PI beads increases effective polarization of the molecules in the wire and resulting in slightly shorter average NN O−O distances.

To investigate the structure of the soft water wires, the $P(R_{O-O})$ distribution functions were separately calculated for the inner and outer NN O−O pair distances of each complex and presented in Figure 6 for the classical CP trajectories (since there is little difference between the CP and PICP distributions, the latter quantum distributions were omitted). The first two peaks represent the distribution of the inner water molecules in both complexes and the maximum of both peaks are close at ≈2.45 and ≈2.5 Å for the tetramer and pentamer, respectively. The structures between the two differ: the tetramer complex

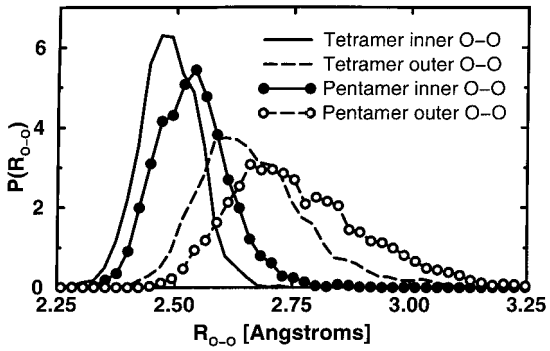

Figure 6. Distribution functions $P(R_{OO})$ of the inner and outer nearest neighbor (NN) oxygen−oxygen water distances in the soft tetramer and pentamer complexes for classical CP trajectories at 300 K.

has a sharper peak that rises and decays more rapidly than the corresponding pentamer peak, which is shorter and broader. The outer O−O NN distances for both complexes are shifted further out in distance and centered at ≈2.6 and ≈2.7 Å for the tetramer and pentamer, respectively. The peak densities at larger distances >2.8 Å are due to the lack of solvation at the end of the water wires. Thus, the slightly different average inner and outer distances between the soft tetramer and pentamer complexes are also seen in the structural properties, which points to the underlying difference in symmetry between the two complexes.

The hydronium ion, H_3O^+ is common to both soft tetramer and pentamer wire complexes, making its structure of interest. The O−H bonds are classified into three distinct types: non-hydrogen-bonded (NHB) covalent O−H bonds that dangle from the sides of the wire, hydrogen-bonded (HB) covalent O−H bonds that point to the oxygens of edge water molecules, and hydrogen-bonded (HB*) O−H bonds that contain a mobile H* proton. In the soft tetramer, the three types NHB, HB, and HB* are used to classify the O−H bonds associated with H_3O^+,

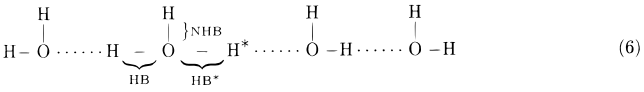

(6)

while in the pentamer, since the center hydronium ion contains two H* protons,

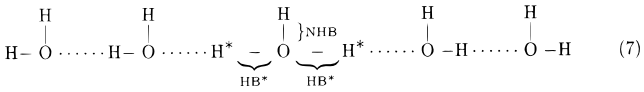

(7)

only the NHB and HB* types apply; the covalent HB O−H bond exists in the NN water molecule, pointing towards and end water of the pentamer. The average values for these O−H bonds in both soft complexes are given in Table 2, where it can be seen that $\langle r^{T}_{HB^*}\rangle \approx 1.25 > \langle r^{P}_{HB^*}\rangle \approx 1.10$. In the tetramer complex, the longer HB* O−H distances correspond to a H* proton sandwiched exactly in the middle of the tetramer, hydrogen bonded on either side to neighboring water molecules, forming the $H_5O_2^+$ species midchain. In the pentamer complex, the somewhat shorter HB* O−H bond distance corresponds to two hyperextended covalent bonds of the H_3O^+ ion that are hydrogen bonded to neighboring water molecules.

The O−H distribution functions for H_3O^+ calculated for classical CP and quantum PICP for both soft tetramer and pentamer complexes are shown in Figures 7 and 8. In the soft tetramer complex, H_3O^+ ions periodically form on either inner water molecule. These contain three types of O−H bonds NHB, HB, and HB* and the corresponding distribution functions

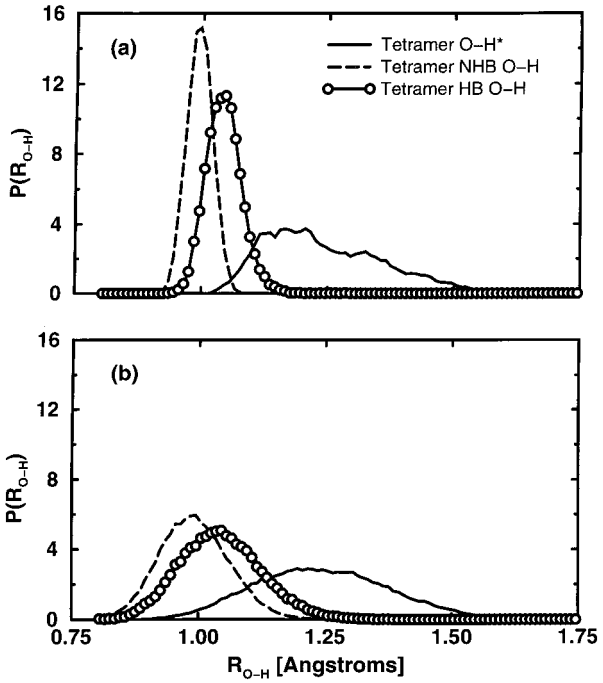

Figure 7. Distribution functions $P(R_{OH})$ for O−H and O−H* type bonds associated with the H_3O^+ in the soft tetramer complex at 300 K: (a) classical CP distributions; (b) quantum nuclear PICP distributions.

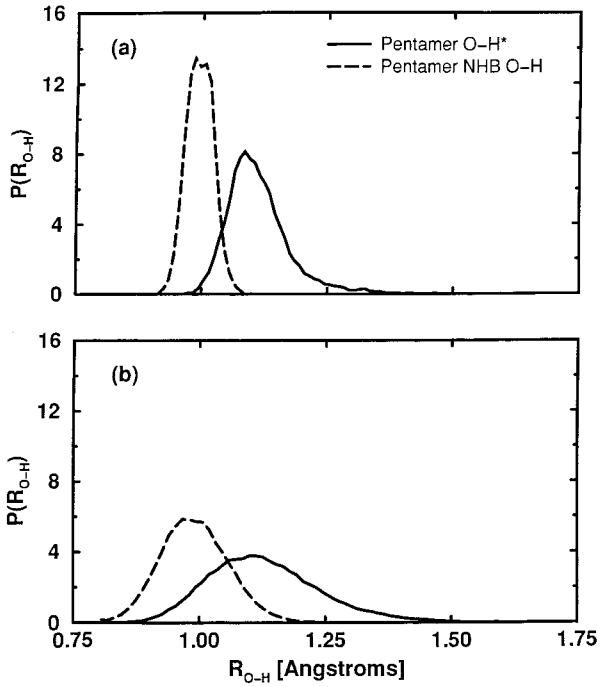

Figure 8. Distribution functions $P(R_{OH})$ for O−H and O−H* type bonds associated with the H_3O^+ in the soft pentamer complex at 300 K: (a) classical nuclear CP distributions; (b) quantum nuclear PICP distributions.

$P(R_{O-H})$ are plotted for both the CP (Figure 7a) and PICP (Figure 7b) cases. The classical and quantum distributions share more or less the same maximum peak values (NHB, ≈0.98 Å; HB, ≈1.05 Å; HB*, ≈1.2 Å), which agree with the average values (see Table 2). The nuclear dispersion due to the path integral treatment of the nuclei in PICP, is reflected in the quantum O−H distribution functions; the same approximate trends in heights and widths of the peak distributions are also seen between corresponding peaks of both classical and quantum

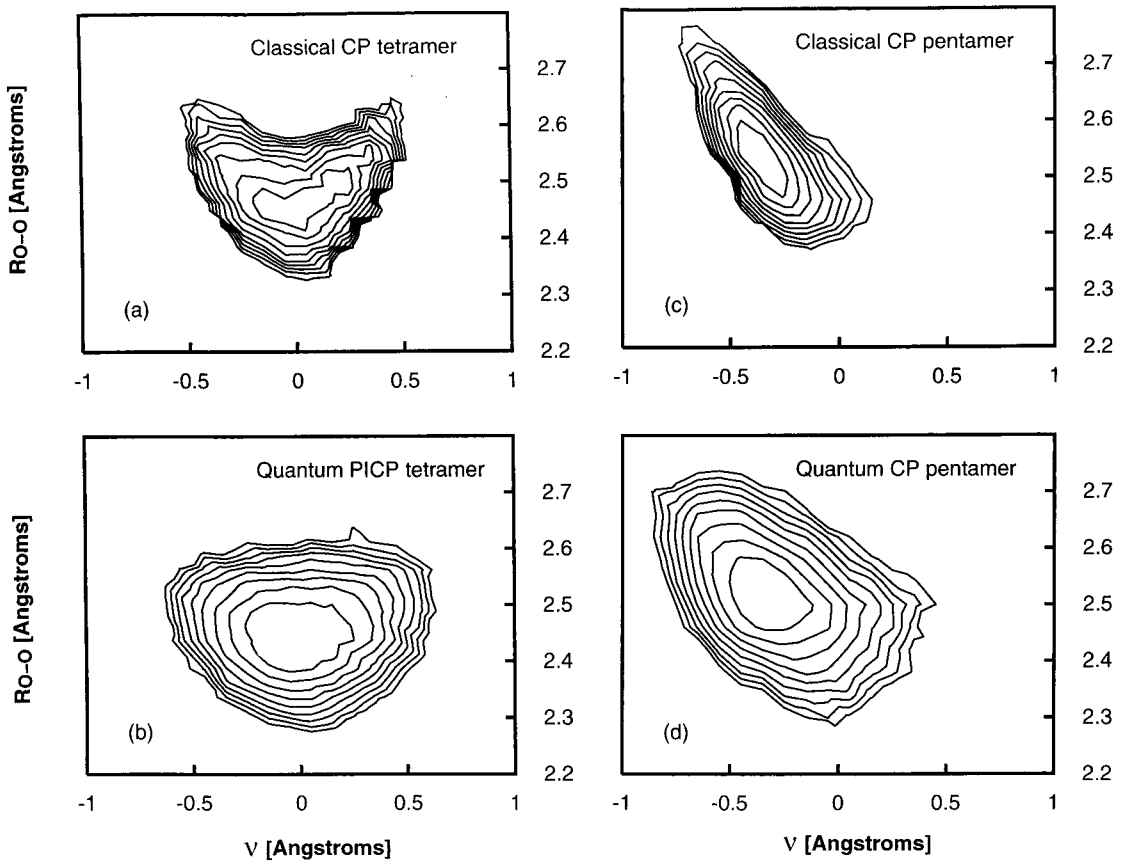

Figure 9. Effective free energy ΔF and potential of mean force PMF surfaces as a function of asymmetric stretch coordinate ν and inner NN R_{OO} distance at 300 K. Classical CP ΔF surfaces are shown for the tetramer (a) and pentamer (c) complexes, and quantum PICP bead PMF surfaces are shown for the tetramer (b) and pentamer (d) complexes, respectively. Contour lines are shown in increments of 0.2 kcal/mol from 0 to 2 kcal/mol.

distributions. The two covalent O−H bonds, NHB and HB, give the first two peaks in the distribution, where the former NHB O−H is of greatest height, occurring at the shortest distances, and the latter HB O−H is slightly shifted outward in distance with a broader distribution due to hydrogen bonding with an end water. The final HB* O−H peak, distributed over 0.5 Å, is the most broad, illustrating the H_3O^+ and $H_5O_2^+$ ions that occur in proton transfer between the two NN inner water molecules. The pentamer complex O−H distribution functions for the inner H_3O^+ ion are presented for the CP (Figure 8a) and PICP (Figure 8b) studies; the inner H_3O^+ ion is made up of one covalent NHB O−H bond, dangling off the ion, and two HB* O−H bonds to NN waters. The peak maxima coincide between classical and quantum studies (see Table 2), and the latter quantum distribution again shows the effects of nuclear dispersion. The first pentamer NHB O−H peaks match the distribution of NHB O−H peaks in the tetramer for both classical and quantum studies. The second peak for the pentamer HB* O−H bond at $r = 0.95-1.4$ Å, in comparison to the HB and HB* tetramer O−H bond distributions, is of intermediate height and distance to these tetramer peaks and centered approximately halfway between the two HB and HB* tetramer O−H bond distributions at $r = 1.1$ Å. This indicates that the pentamer HB* O−H bond, although mostly hyperextended in long covalent bonds, can also contract to shorter covalent lengths as well as extend to even longer lengths at $r \approx 1.2$ Å, reminiscent of those found for the $H_5O_2^+$ species. At this value of $r \approx 1.2$ Å, the distribution has already decayed to a fraction of its maximum value, indicating that O−H* bonds of the $H_5O_2^+$ type form infrequently. Full proton transfer in the pentamer, which forms a neighboring off-center, fully covalent H_3O^+ ion, seems to be an even more infrequent classical event, since there is very little peak density at corresponding longer O−H lengths. However, the tails of the HB* O−H bonds persist in the quantum distributions so that nuclear dispersion may aid in the formation of off-center covalent NN H_3O^+ ions in the pentamer complex.

As is the case in the average values between hard and soft potentials, the structural hard and soft distribution functions are similar. Thus the biggest difference between the hard and soft models is the asymmetric minima found for the tetramer complex. The soft tetramer asymmetries are washed out at finite temperatures, suggesting that proton transfer is a frequent event and the proton transfer barrier must be less than k_BT.

B. Effective Free Energy and Potential of Mean Force Profiles. The effective free energy and potential of mean force surfaces for the asymmetric stretch ν as a function of intermolecular NN distances R_{O-O} are shown in Figure 9 for the soft tetramer and pentamer. The surfaces for the hard complexes are omitted since they show no appreciable differences. The asymmetric stretch coordinate serves as a reaction coordinate for the proton transfer and is defined as

$$\nu = r_{O_aH^*} - r_{O_bH^*} \tag{8}$$

where O_a and O_b are the oxygens of NN water molecules a and b, which confine the mobile proton H*. This choice of a localized asymmetric stretch serving as a reaction coordinate may not be ideal, especially in the case of the PICP complexes where a proton can appear delocalized over two bonds (for example, see Figure 5b). However, as these events are rare, the asymmetric stretch coordinate should be useful in analysis of individual localized proton motion between NN water molecules.

The effective free energy surfaces are obtained from

$$\Delta F(R_{O-O},\nu) = -k_B T \ln[P(R_{O-O},\nu)] \quad (9)$$

where $P(R_{O-O},\nu)$ is the two-dimensional distribution function for the O−O distances R_{O-O} and proton asymmetric stretch coordinate ν. In the tetramer complex, the coordinates of the two inner water molecules were used to generate ΔF, while in the pentamer, the two inner NN water pairs included the middle and designated right water pairs to generate ΔF. The free energy surfaces are presented in Figures 9a,c for the soft CP complexes. For the PICP studies, the distinction is made that the potential of mean force (PMF) (shown in Figures 9b,d), is obtained from the path integral bead distribution in eq 9; the correct quantum effective free energy surfaces should be computed from the path integral centroid distributions. In the classical case ($P = 1$), the ΔF and the PMF surfaces are the same. All surfaces are plotted at contour levels of 0.2 kcal/mol.

The soft tetramer complex ΔF and PMF surfaces are shown for the CP (Figure 9a) and PICP (Figure 9b) studies and minima in both cases are found at ($\nu = 0$ Å, $R_{O-O} = 2.45$ Å). Both surfaces appear shallow, allowing the proton to move freely between the inner water molecules and, as expected, quantum nuclear dispersion further broadens the PMF surface, washing out the slight structure seen at longer R_{O-O} bond lengths.

Free energy surfaces and PMFs for the soft pentamer complex are dramatically different from the tetramer complex. Immediately noticeable is the strong asymmetry at $\nu = 0$, compared to the tetramer complex, whose surface is centered at $\nu = 0$. The minima in the surfaces occur at negative ν coordinates at $R_{O-O} = 2.5$ Å (Figures 9c,d), corresponding to the protons on right sides of the inner hydronium ion. This reinforces the observations that the pentamer H* protons make very few excursions to bind with NN water molecules, as illustrated in the classical case where no well is found at the zero asymmetric stretch coordinate and on the opposite side of the surface (see Figure 9c). In the quantum PICP calculations, the pentamer PMF surfaces have been again broadened due to nuclear dispersion and corresponding energy contour levels extend farther into opposite positive asymmetric stretch regions.

C. Comparison to the Work of Pomès and Roux. Pomès and Roux have studied quantum water wires consisting of an excess proton up to nine water molecules in vacuum[15,16] and in realistic biological media.[20,21] These authors used the dissociable PM6 polarization model[26,27] of water in classical and path integral simulations and showed that, as the O−O separation involving the transferring proton was increased, the model gave a much steeper potential barrier for proton transfer than that obtained from Hartree−Fock (HF/4-31G) calculations. As noted earlier, the PM6 model overestimates the barrier height, an artifact of the neglect of electron correlation at the HF level of theory, thus predicting an artificially high barrier to proton transfer through water hydrogen bonds.[42,73]

Despite the drawbacks in the PM6 model, our results suggest that Pomès and Roux have indeed captured the qualitative features of proton transfer that distinguish the tetramer and pentamer complexes from one another. Our soft complexes correspond to the complexes studied by these authors. They first observed the transfer of the excess proton H*, forming H_3O^+ and $H_5O_2^+$ ions, with the inner two water molecules of the tetramer complex and also the hyperextended O−H* bonds of the middle H_3O^+ ion solvated in the pentamer complex. Although we find a slightly asymmetric geometry minimum while they find a symmetric one, good agreement with the results of these authors is obtained for average O−O and O−H pair distances reported for both complexes.

Our results begin to differ at the quantitative level, which is most easily seen in the comparison of our ΔF and PMF surfaces to those calculated by Pomès and Roux.[15,16] Although the PMF surface is based on the O−H distances rather than the asymmetric stretch coordinate, this will not affect the energy differences in the surface based on the NN O−O distance; we can estimate the corresponding O−H surface minima in the PMF surfaces from the maxima in our calculated $P(R_{O-H})$ functions from Figures 7 and 8 for the proton H*. To facilitate comparison, the ΔF and PMF surfaces in Figure 9 have been plotted at the corresponding PMF energy contour levels of 0.2 kcal/mol.

On the basis of the good agreement in average structural properties between the two studies for the tetramer, it is not surprising that the minima in both surfaces agree. However, upon further inspection, of both classical surfaces, we note that the PMF surfaces increase in energy much more sharply away from the global minimum. For instance, at short O−O distances of $R_{O-O} \approx 2.4$ Å and $\nu = 0$, we are still within one contour level from the minimum, while the PMF surfaces are already five to six contour levels above the minimum, corresponding to an energy discrepancy on the order of 1 kcal/mol. At larger O−O distances, the converse is true, where at $R_{O-O} \approx 2.6$ Å and $\nu = 0$ Å, the last contour level at 2 kcal/mol has been reached. This faster rise in free energies, especially at shorter distances, is the most striking difference between the two studies and seems to indicate that, overall, the PM6 model may be too repulsive beyond the minimum distances in the energy surfaces. Finally, in the pentamer complexes, the global minimum in the PM6 surface is at a longer distance of 2.65 Å, while the present results suggest a distance of ≈2.50 Å. Thus, the overall distribution functions will be quite different.

D. EVB Model Calculations. Distribution functions involving longer time scale motion, such as bending and torsional motions of the water wire backbone are computationally expensive to converge using CP or PICP methods. Thus the empirical valence bond (EVB) model[74] of Sagnella and Tuckerman,[73] analytically fit to *ab initio* potential energy surfaces that included electron correlation at the MP2 level, was used to provide an empirical adiabatic surface for the $H_5O_2^+$ complex within the water wires.

Classical and quantum path integral molecular dynamics were performed using the EVB model in the soft confining potential only. Comparison between pair distribution functions obtained for the classical EVB and the DFT CP studies showed minor discrepancies between the maxima in the O−O and O−H pair distribution functions, where the EVB model gave slightly smaller values, indicating that the EVB $H_5O_2^+$ is more compact (this finding is consistent with the reported results in ref 73 for the gas phase $H_5O_2^+$). Nevertheless, the differences are minor (≈0.1 Å) in the classical studies and comparison between the path integral EVB and CP studies shows broadened distribution functions from nuclear dispersion, further mitigating differences between the two models.

The inner and outer asymmetric stretches imaginary time correlation functions $\nu^2(\tau)$ were calculated for the path integral EVB, soft and hard PICP studies and presented in Figure 10. In all models, the trends are qualitatively the same, where the inner asymmetric stretch correlation functions exhibit a sharper rise compared to the outer asymmetric stretches, which have a smaller slope and broad plateau region. Thus the outer asymmetric stretches are more confined, while the inner asymmetric stretches are less confined and more free particle-like. These

results reflect the fact that the proton transfers primarily between the two inner water molecules in all the models. On the basis of the pair distribution functions and imaginary time mean-squared displacement, we are satisfied that the EVB model will give qualitatively reasonable results for the angular distribution functions.

In Figure 11a, the torsional angle φ distribution functions are presented for the EVB quantum path integral tetramer for the torsions involving the backbone oxygens φ_{OOOO}, and the two H−O−O−H torsions φ_{HOOH} that comprise the inner and outer two water molecules. The atoms involved in the torsional angles are identified in bold within square brackets.

$$\varphi_{OOOO}: \mathrm{H-[O]\cdots H-[O]-H^*\cdots[O]-H\cdots[O]-H}$$

$$\text{Inner } \varphi_{HOOH}: \mathrm{H-O\cdots H-[O]-H^*\cdots[O]-H\cdots O-H}$$

$$\text{Outer } \varphi_{HOOH}: \mathrm{H-[O]\cdots H-[O]-H^*\cdots O-H\cdots O-H} \qquad (10)$$

Since the classical and quantum distributions were similar, only the quantum distributions are presented in Figure 11a. The O−O−O−O torsion is peaked at 180° and contains regions of zero density, indicating the O−O−O−O backbone does not fully rotate about its axis. The inner H−O−O−H torsion also peaks at 180° but does contain some density at all angles in contrast to the outer H−O−O−H torsion, which has uniform density at all angles. These results show that the end water molecules spin freely while the angular motion of the inner waters are constrained, due to stronger hydrogen bonding.

The quantum bend angle θ distribution functions for the O−O−O, inner O−H*−O and outer O−H−O bending angles are shown in Figure 11b, and the atoms involved in the bending angles are identified within square brackets.

$$\theta_{OOO}: \mathrm{H-[O]\cdots H-[O]-H^*\cdots[O]-H\cdots O-H}$$

$$\text{Inner } \theta_{OH^*O}: \mathrm{H-O\cdots H-[O]-[H]^*\cdots[O]-H\cdots O-H}$$

$$\text{Outer } \theta_{OHO}: \mathrm{H-[O]\cdots[H]-[O]-H^*\cdots O-H\cdots O-H} \qquad (11)$$

The broadest θ_{OOO} distribution peaked at 120°. There were observed differences between the types of O−H−O bend angle distributions, where the narrower inner θ_{OH^*O} bend angle density peaked at 175° while outer θ_{OHO} bend distribution peaked at 170°. Although the classical distributions were unchanged for the θ_{OOO} and θ_{OHO} angles, the classical distribution for the θ_{OH^*O} bend was slightly narrower, but peaked at the same position as in the quantum case. Thus, in comparing the classical to quantum angular distribution, the quantum treatment of the nuclei only affects the transferring proton θ_{OH^*O} bend angle, broadening the quantum distributions slightly.

E. Capped Solvation of Water Wires. In the unsolvated tetramer and pentamer complexes, proton transfer took place primarily between two or three neighboring, inner water sites. The proton was never observed to transfer between outer water sites. Thus, studies were performed where a tetramer water wire was capped with water caps to solvate both wire ends. During CP molecular dynamics, the proton was observed to be more mobile, traversing the entire length of the wire and occasionally migrating into the cap regions. These events are shown in a series of instantaneous snapshots and presented in Figure 12.

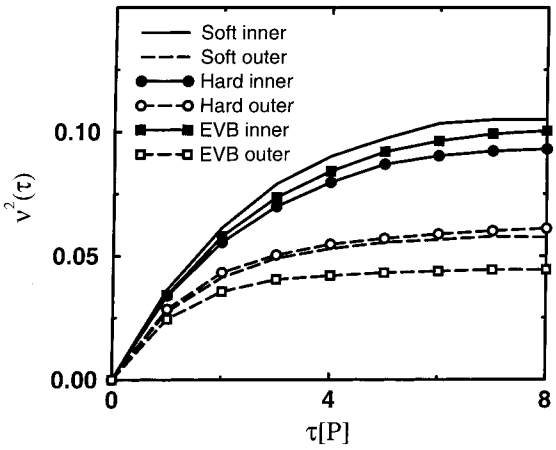

Figure 10. Imaginary time asymmetric stretch correlation functions for the PI-EVB and PICP tetramer complexes at 300 K, showing the inner and outer asymmetric stretch correlation functions.

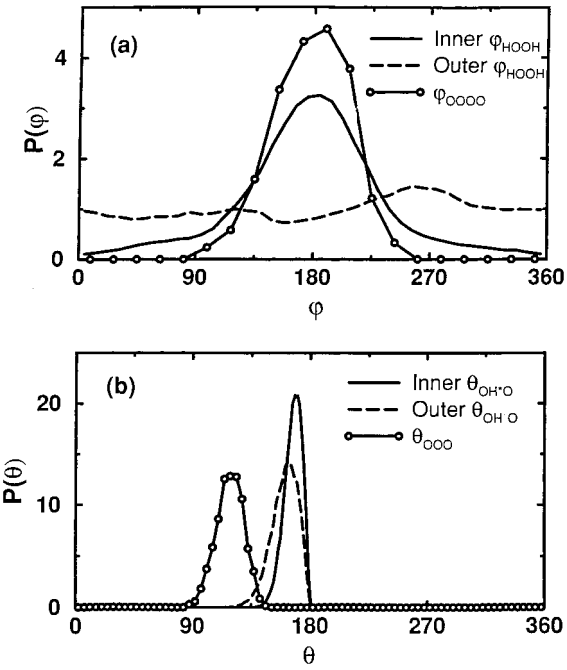

Figure 11. Effective valence bond EVB path integral angular distributions for the soft tetramer at 300 K are shown for (a) torsional angle, φ, and (b) bend angle, θ. Atoms involved in torsional and angular angles are defined in eqs 10 and 11.

To characterize the proton transfer along the wire, a new coordinate

$$\mathbf{q} = \mathbf{r}_{O_1^*} + S(\mathbf{r}_{O_1^*},\mathbf{r}_{O_2^*},\mathbf{r}_{H^*})\mathbf{r}_{H^*O_1^*} \qquad (12)$$

is presented, which measures the structural diffusion accompanying proton transfer. The transferring proton H* is located between two oxygen water sites O_n^* sites and the nearest oxygen to H* has $n = 1$. A function S is chosen so that the **q** coordinate varies continuously as the proton transfers from one site to another and the hydronium changes identity. The function S is defined as $S(\mathbf{r}_1^*,\mathbf{r}_{O_2^*},\mathbf{r}_{H^*}) = R^2(3 - 2R)$ and $R =$

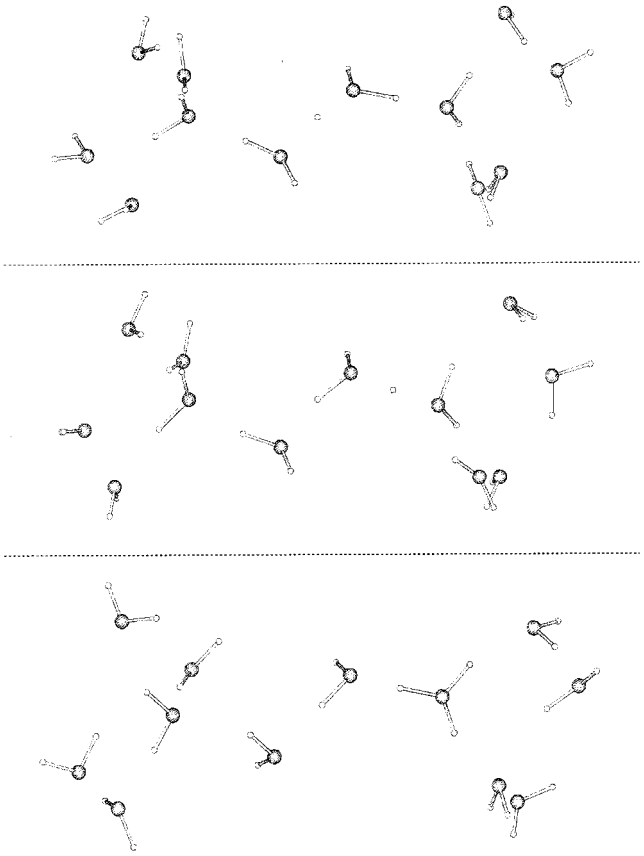

Figure 12. Instantaneous configurations of the cap solvated tetramer water wire complex taken from the CPMD calculation at 300 K. From top to bottom, the proton transfers from the two inner waters pairs to the right outer water pairs and finally forms hydronium at the end solvated water site.

$(|\mathbf{r}_{H^*O_1^*}| - r_c)/(1/2|\mathbf{r}_{O_1^*O_2^*}| - r_c)$ where $r_c = 0.95$ is a constant optimized to give the smoothest evolution of **q**. When the excess proton forms H_3O^+, the **q** coordinate is designed to point to the oxygen of the H_3O^+ group and points to the H* hydrogen when it is located directly between the two oxygens. At all other locations of H*, **q** points to a location between H* and the closest oxygen and, in this way, follows the structural diffusion process in a continuous manner. A schematic of the switching function is presented in Figure 13, displaying from top to bottom, the **q** coordinate following the structural diffusion.

The **q** coordinate was first calculated for the unsolvated soft tetramer and pentamer complexes. Since the proton transfer occurred along the channel axis, the coordinates projected along the *z*-dimension were used for analysis. In Figure 14a, the instantaneous values were plotted for the q_z, $z_{O_1^*}$, and z_{H^*} for a selected time interval of 0.5 ps. The z_{H^*} coordinate showed the frequent proton transfer between the two inner water molecules. The $z_{O_1^*}$ coordinate switched identity between the two inner water sites and the q_z coordinate was seen to continuously follow the structural diffusion. The pentamer complex is presented in Figure 14b where the z_{H^*} switched identity between the HB protons attached to the H_3O^+ at the center of the pentamer. The $z_{O_1^*}$ mostly remained on the inner H_3O^+ oxygen, but switches did occur to the outer neighboring water oxygens. As in the tetramer, the pentamer q_z coordinate followed the structural diffusion.

The z-components are presented for the solvated water wire in Figure 15 where the proton has diffused from the inner to outer water sites, as seen in Figure 12. The instantaneous components plotted together for 1 ps show features observed in both

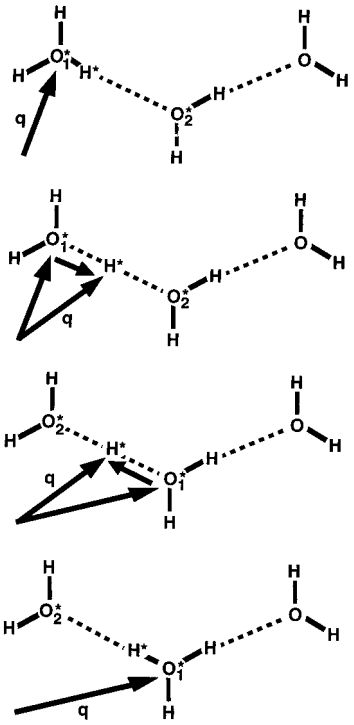

Figure 13. Schematic showing the **q** transfer coordinate (see text for definition) that continuously follows the structural diffusion that accompanies the proton transfer along the water wire. From top to bottom, the proton begins attached to the left water site as H_3O^+ and then begins to transfer to the middle water. As the proton moves to the middle water site, the O_1^* and O_2^* switch change identity and finally the proton attaches to the middle water to form H_3O^+.

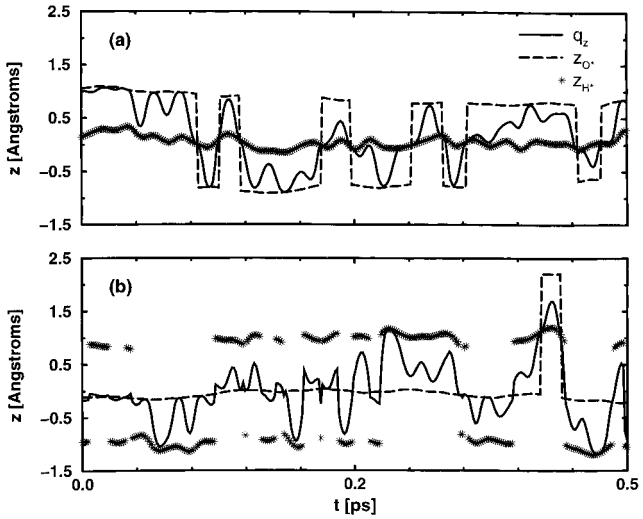

Figure 14. Instantaneous *z*-components **q**, H*, and O_1^* of the unsolvated (a) tetramer and (b) pentamer complexes, showing the change in identity of the transferring proton H* and nearest oxygen O_1^* and the coordinate **q** that continuously follows the structural diffusion, for a representative 0.5 ps CP trajectory at 300 K.

the unsolvated tetramer and pentamer complexes. Initially, to 0.4 ps, the z_{H^*} switched identity between HB protons on either side of H_3O^+ as in the pentamer complex. Then a short period occurred between 0.4 and 0.6 ps, where the proton transferred back and forth between two water sites as in the tetramer complex. Finally, attachment to an end water site formed a new H_3O^+ after 0.6 ps and z_{H^*} switched identity between the two HB protons on either side of the new H_3O^+. The $z_{O_1^*}$ coordinate reflected the switching of oxygen identities and the q_z coordinate followed the structural diffusion continuously.

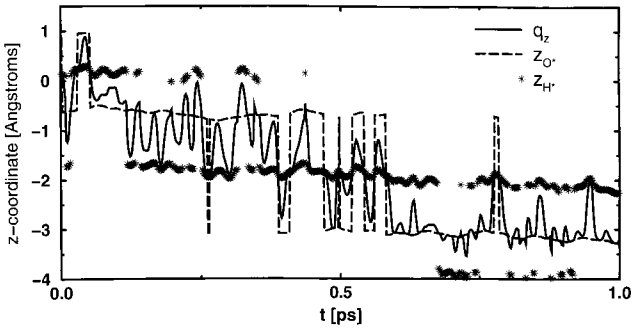

Figure 15. Instantaneous *z* components **q**, H*, and O_1^* of the capped tetramer, showing the change in identity of the transferring proton H* and nearest oxygen O_1^* and the coordinate **q** that continuously follows the structural diffusion, for a representative 1 ps CP trajectory at 300 K.

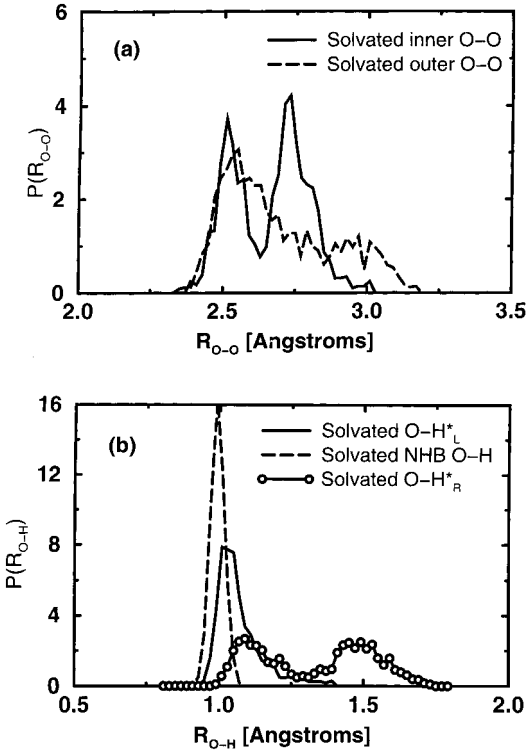

Figure 16. Pair distribution functions, (a) $P(R_{OO})$ and (b) $P(R_{OH})$ for the capped tetramer from CP calculations at 300 K.

The pair distribution functions for the inner and outer pairs distribution functions are presented for the classical solvated species in Figure 16a. Movement of the proton from the inner to outer O−O pairs is reflected in the distributions. The inner O−O peak is now binodal; the first peak reflects the O−O distances when H* is contained between the two inner water sites, while the second shows the expansion of inner O−O distances as H* moves to the next outer pair. The binodal character is not as dramatic in the outer O−O pairs, but density does exist at shorter distances, reflecting the prescence of H* between the outer O−O pairs. In Figure 16a, the O−H pairs distributions are plotted for the solvated species. Since the proton is more mobile, the water site that the H* hops onto and jumps off from is considered as O, while H_L^* is the proton that hops and H_R^* denotes the proton that jumps. In this set of distributions, NHB O−H resembles the distribution functions for the tetramer and pentamer complexes in Figures 7 and 8. The O−H_L^* distribution has a long tail to 1.4 Å, which shows the approach of the H_L^* from a neighboring water molecule; the density at ∼1.1 Å reflects the attachment of H_L^* as a HB O−H group. The O−H_R^* distribution shows density at short distances ∼1.1 Å representing the bonding of the H_R^*; the density at greater distances represents the H_R^* jump from the O group to form H_3O^+ at the end of the tetramer.

IV. Conclusion

Ab initio MD was used to investigate two linear water wire complexes composed of an excess proton and either four or five molecules placed in cylindrical confining potentials that mimic a channel. In the tetramer complex, the proton shuttled between the two inner neighboring water molecules, forming alternating H_3O^+ and $H_5O_2^+$ ions. By contrast, in the pentamer species, proton transfer between nearest neighbor waters was a rare event with an H_3O^+ ion stablized in the middle of the wire and two hyperextended covalent bonds pulled in competition by neighboring hydrogen-bonded water molecules.

The geometric minima were obtained for complexes in both a soft and hard confining potential. The soft potential gave a slightly asymmetric minimum as opposed to the hard potential symmetric minimum. However, the asymmetry in the soft tetramer minimum was washed out at finite temperatures where the soft and hard average equilibrium NN pair distances were in agreement with one another. Overall, the soft complexes were slightly more angular and compact since the inner water sites could penetrate further into the soft cylindrical confining potential. Between tetramer and pentamer complexes, differences in averaged properties were revealed only in the different O−H* lengths, which illustrated the different proton transfer processes observed. Further investigation into the structures of the complexes revealed shifts in O−O NN peaks and a radically different structure of the hydronium ion was present in each complex.

The effects of incorporating nuclear quantum effects via path integrals was clearly seen in the O−H distribution functions. Also, the PICP systems have slightly smaller average NN O−O distances. In the quantum pentamer complex, protons were observed to delocalize over three NN water sites to form extended complexes such as $H_7O_3^+$, and no proton transfer was observed between outer water sites. Thus, it would be interesting to increase the chain length and search for even larger extended ionic species where the proton is possibly delocalized over more water sites.

Pomès and Roux previously presented work on the same water wire systems using an empirical potential. They characterized the differences in the proton translocation between the tetramer and pentamer water complexes. Careful comparison to their equilibrium properties revealed good agreement in most cases, but quantitative differences in ΔF and PMF surfaces for the proton transfer were apparent.

Calculations using a model EVB surface were also performed to characterize bending and torsional motions of the water wire backbone, which are computationally expensive to converge using CP or PICP methods. There appeared to be little difference between the quantum and classical torsional distributions. The φ_{OOOO} and inner φ_{HOOH} were peaked at 180°, while the outer φ_{HOOH} torsional distributions were featureless, indicating that the end waters rotated freely about their torsional axes. The bend angle distributions were also similar between the classical and quantum cases, with a slight quantum dispersion seen only in a softening θ_{OH^*O} bend distributions. Analysis of the imaginary time mean-squared displacement for the asymmetric stretch $\nu^2(\tau)$, for PI-EVB and PICP models showed that the inner

asymmetric stretches, containing the transferring proton H* were much less confined than the outer asymmetric stretches.

Capping waters were added to the end of the tetramer complex to investigate the effects of end solvation on the proton transfer process. Contrary to the case in vacuum, where the excess proton only transferred between the inner two water molecules, the excess proton was observed to transfer between the inner water sites and continue onto the outer water sites where a solvated H_3O^+ formed in the capping regions. Calculated distribution functions revealed proton transfer across several water sites. A coordinate **q** (cf. eq 12) was employed to follow the structural diffusion along the water wire.

Overall, our studies suggest that nuclear quantum effects play a relatively minor role in the small linear clusters. While it is unlikely that the addition of capping water and/or a biologically realistic environment will change dramatically the importance of quantum effects on the actual proton transfer process through a single H-bond, these additions may complicate the mechanism of proton transfer and could therefore bring in quantum effects in other ways, e.g., increased delocalization over the length of the wire of the type observed in the pentamer case. Such studies are reserved for future work.

Acknowledgment. This research was supported by generous grants from the National Institutes of Health and the National Science Foundation. D.E.S. acknowledges support from NIH postdoctoral fellowship F32-GM19273-01. The calculations were performed either on site at the Center for Molecular Modeling or at the Cornell and Maui supercomputing centers using the IBM SP2 parallel machines. We thank Sundaram Balasubramanian and Ken Bagchi for their helpful comments and David Coker for his critical review of the manuscript.

References and Notes

(1) Copeland, R. A.; Chan, S. I. *Annu. Rev. Phys. Chem.* **1989**, *40*, 671.
(2) Rawn, J. D. *Biochemistry*; Neil Patterson Publishers: Burlington, NC, 1989.
(3) Nagle, J. F.; Tristram-Nagle, S. *J. Membr. Biol.* **1983**, *74*, 1.
(4) Stowell, M. H. B.; McPhillips, T. M.; Rees, D. C.; Soltis, S. M.; Abresch, E.; Feher, G. *Science* **1997**, *276*, 812.
(5) Lancaster, C. R. D.; Michel, H. *Photosynth. Res.* **1996**, *48*, 65.
(6) Ermler, U.; Fritzsch, G.; Buchanan, S. K.; Michel, H. *Structure* **1992**, *10*, 925.
(7) Deisenhofer, J.; Epp, O.; Sinning, I.; Michel, H. *J. Mol. Biol.* **1995**, *246*, 429.
(8) Baciou, L.; Michel, H. *Biochemistry* **1995**, *34*, 7967.
(9) Hille, B. *Ionic Channels of Excitable Membranes*; Sinauer: Sunderland, MA, 1984.
(10) Martinez, S. E.; Huang, D.; Ponomarev, M.; Cramer, W. A.; Smith, J. L. *Protein Sci.* **1996**, *5*, 1081.
(11) Papadopoulos, G.; Dencher, N. A.; Zaccaï, G.; G. Büldt. *J. Mol. Biol.* **1990**, *214*, 15.
(12) Akeson, M.; Deamer, D. W. *Biophys. J.* **1991**, *60*, 101.
(13) Deamer, D. W.; Akeson, M. *Adv. Chem. Ser.* **1995**, *235*, 41.
(14) Pebay-Peyroula, E.; Rummel, G.; Rosenbusch, J. P.; Landau, E. M. *Science* **1997**, *277*, 1676.
(15) Pomès, R.; Roux, B. *Chem. Phys. Lett.* **1995**, *234*, 416.
(16) Pomès, R.; Roux, B. *J. Phys. Chem.* **1996**, *100*, 2519.
(17) Drukker, K.; Hammes-Schiffer, S. *J. Chem. Phys.* **1997**, *107*, 363.
(18) Decornez, H.; Drukker, K.; Hurley, M. M.; Hammes-Schiffer, S. *Ber. Bunsen-Ges. Phys. Chem.* **1998**, *102*, 533.
(19) Chiu, S.-W.; Subramaniam, S.; Jakobsson, E.; McCammon, J. A. *Biophys. J.* **1989**, *56*, 253.
(20) Pomès, R.; Roux, B. *Biophys. J.* **1996**, *70*, A263.
(21) Pomès, R.; Roux, B. *Biophys. J.* **1996**, *71*, 19.
(22) Sagnella, D. E.; Voth., G. A. *Biophys. J.* **1996**, *70*, 2043.
(23) Sagnella, D. E.; Laasonen, K.; Klein, M. L. *Biophys. J.* **1996**, *71*, 1172.
(24) Roux, B.; Karplus, M. *Annu. Rev. Biophys. Biomol. Struct.* **1994**, *23*, 731.
(25) Car, R.; Parrinello, M. *Phys. Rev. Lett.* **1985**, *55*, 2471.
(26) Stillinger, F. H.; David, C. W. *J. Chem. Phys.* **1978**, *69*, 1473.
(27) Weber, T. A.; Stillinger, F. H. *J. Phys. Chem.* **1982**, *86*, 1314.
(28) Halley, J. W.; Rustad, J. R.; Rahman, A. *J. Chem. Phys.* **1993**, *98*, 4110.
(29) Tuckerman, M. E.; Marx, D.; Klein, M. L.; Parrinello, M. *Science* **1997**, *275*, 817.
(30) Laasonen, K.; Sprik, M.; Parrinello, M.; Car, R. *J. Chem. Phys.* **1993**, *99*, 9081.
(31) Sprik, M.; Hutter, J.; Parrinello, M. *J. Chem. Phys.* **1996**, *105*, 1142.
(32) Tuckerman, M.; Laasonen, K.; Sprik, M.; Parrinello, M. *J. Phys. Chem.* **1995**, *99*, 5749.
(33) Tuckerman, M.; Laasonen, K.; Parrinello, M. *J. Chem. Phys.* **1995**, *103*, 150.
(34) Soper, A. K.; Bruni, F.; Ricci, M. A. *J. Chem. Phys.* **1997**, *106*, 247.
(35) Soper, A. K. *Chem. Phys.* **1986**, *107*, 47.
(36) Meibroom, S. *J. Chem. Phys.* **1961**, *34*, 375.
(37) Feynman, R. P. *Statistical Mechanics*; Benjamin: Reading, MA, 1972.
(38) Feynman, R. P.; Hibbs, A. R. *Quantum Mechanics and Path Integrals;* McGraw-Hill: New York, 1965.
(39) Marx, D.; Parrinello, M. *J. Chem. Phys.* **1996**, *104*, 4077.
(40) Tuckerman, M. E.; Marx, D.; Klein, M. L.; Parrinello, M. *J. Chem. Phys.* **1996**, *104*, 5579.
(41) Tuckerman, M. E.; Ungar, P. J.; von Rosenvinge, T.; Klein, M. L. *J. Phys. Chem.* **1996**, *100*, 11878.
(42) von Rosenvinge, T.; Tuckerman, M. E.; Klein, M. L. *J. Chem. Soc., Faraday Disscuss.* **1997**, *106*, 279.
(43) Benoit, M.; Marx, D.; Parrinello, M. *Comp. Mater. Sci.* **1998**, *10*, 88.
(44) Benoit, M.; Marx, D.; Parrinello, M. *Nature* **1998**, *392*, 258.
(45) Rousseau, R.; Marx, D. *Phys. Rev. Lett.* **1998**, *80*, 2574.
(46) Marx, D.; Parrinello, M. *Nature (London)* **1995**, *375*, 216.
(47) Marx, D.; Parrinello, M. *Science* **1996**, *271*, 179.
(48) Hohenberg, P.; Kohn, W. *Phys. Rev. B* **1964**, *136*, 864.
(49) Kohn, W.; Sham, L. J. *Phys. Rev. A* **1965**, *140*, 1133.
(50) Stich, I.; Car, R.; Parrinello, M.; Baroni, S. *Phys. Rev. B* **1989**, *39*, 4997.
(51) Galli, G.; Parrinello, M. *Phys. Rev. Lett.* **1992**, *24*, 3547.
(52) Mauri, F.; Galli, G. *Phys. Rev. B* **1994**, *50*, 4316.
(53) Tuckerman, M. E.; Parrinello, M. *J. Chem. Phys.* **1994**, *101*, 1302, 1316.
(54) Martyna, G. J.; Klein, M. L.; Tuckerman, M. E. *J. Chem. Phys.* **1993**, *98*, 2796.
(55) Martyna, G. J.; Klein, M. L. Submitted to *J. Chem. Phys.*
(56) Sprik, M. *J. Chem. Phys.* **1991**, *95*, 2283.
(57) Blöchl, P. E.; Parrinello, M. *Phys. Rev. B* **1992**, *45*, 9413.
(58) Marx, D.; Parrinello, M. *Z. Phys. B (Rapid Note)* **1994**, *95*, 143.
(59) Parrinello, M.; Rahman, A. *J. Chem. Phys.* **1984**, *80*, 860.
(60) de Raedt, B.; Sprik, M.; Klein, M. L. *J. Chem. Phys.* **1985**, *80*, 5719.
(61) Hall, R. W.; Berne, B. J. *J. Chem. Phys.* **1984**, *81*, 3641.
(62) Tuckerman, M. E.; Berne, B. J.; Martyna, G. J.; Klein, M. L. *J. Chem. Phys.* **1992**, *97*, 2635.
(63) Pollock, E. L.; Ceperley, D. M. *Phys. Rev. B* **1984**, *30*, 2555.
(64) Sprik, M.; Klein, M.; Chandler, D. *J. Chem. Phys.* **1985**, *83*, 3942.
(65) Sprik, M.; Klein, M.; Chandler, D. *Phys Rev. B* **1985**, *31*, 4234.
(66) Coker, D. F.; Thirumalai, D.; Berne, B. J. *J. Chem. Phys.* **1987**, *86*, 5689.
(67) Barnett, R. N.; Landman, U. *Phys. Rev. B* **1993**, *48*, 2081.
(68) Kohn, W.; Becke, A. D.; Parr, R. G. *J. Phys. Chem.* **1996**, *100*, 12974.
(69) Becke, A. D. *Phys. Rev. A* **1988**, *38*, 3098.
(70) Lee, C.; Yang, W.; Parr, R. G. *Phys. Rev. B* **1988**, *37*, 785.
(71) Xie, Y.; Remington, R. B.; Schaefer, H. F., III. *J. Chem. Phys.* **1994**, *101*, 4878.
(72) Troullier, N.; Martins, J. L. *Phys. Rev. B* **1991**, *43*, 1993.
(73) Sagnella, D. E.; Tuckerman, M. E. *J. Chem. Phys.* **1998**, *108*, 2073.
(74) Warshel, A.; Weiss, R. M. *J. Am. Chem. Soc.* **1980**, *102*, 6218.
(75) Flyvbjerg, H.; Petersen, H. G. *J. Chem. Phys.* **1989**, *91*, 461.